Heliyon

The effects of blend ratio and storage time on thermoplastic starch/poly(butylene adipate-*co*-terephthalate) films

Ray Anne Garalde [a], **Ranumas Thipmanee** [a,b], **Piyawanee Jariyasakoolroj** [a,b], **Amporn Sane** [a,b,*]

[a] *Department of Packaging and Materials Technology, Faculty of Agro-Industry, Kasetsart University, Bangkok 10900, Thailand*

[b] *Center for Advanced Studies for Agriculture and Food, KU Institute for Advanced Studies (CASAF, NRU-KU, Thailand), Kasetsart University, Bangkok 10900, Thailand*

[*] Corresponding author.
E-mail address: amporn.s@ku.ac.th (A. Sane).

Abstract

The objective of this work was to investigate blend ratio and storage time effects on the morphological, mechanical, and thermal properties of thermoplastic starch/poly(butylene adipate-*co*-terephthalate) (TPS/PBAT) films. TPS was prepared from plasticized cassava starch using a twin-screw extruder. TPS was subsequently melt-blended with PBAT with varied weight ratios (i.e., 20/80, 40/60 and 60/40) and blown to form TPS/PBAT films. It was found that increasing the TPS/PBAT ratio to 40/60 led to improved distributions of polymeric components and increased PBAT crystallization temperatures while reducing TPS melting transitions and tensile properties of TPS/PBAT films.

After three months of storage at 30 °C, the tensile strength and secant modulus at 2% strain of TPS/PBAT films increased due to recrystallization of both TPS and PBAT. Blend ratios were the primary determinant for changes in TPS/PBAT film elongation at break with this storage time. Elongation at break decreased at low TPS:PBAT ratios (i.e., 20/80) and increased at high blend ratios (i.e., 60/40). The recrystallization of both TPS and PBAT components were observed from

XRD and DSC analyses. Results obtained from both techniques confirmed the formation of additional crystalline structures of individual components during storage. The recrystallization phenomena also affected thermal transition temperatures of blend components. The crystallization temperature of PBAT-rich phase increased as starch could act as nucleating sites for PBAT. Using DMA, the *tan δ* curve of TPS/PBAT film exhibited two sharp individual peaks corresponding to the glass transitions of PBAT-rich and starch-rich phases. The *tan δ* of TPS-rich phase shifted to higher temperature due to recrystallization of TPS-rich phase.

Keywords: Materials chemistry, Materials science, Chemical engineering

1. Introduction

Blending biodegradable polyesters with thermoplastic starch (TPS) can improve overall mechanical and water resistance properties [1, 2]. Many studies have been conducted on the potential advantages of blending TPS with biodegradable polyesters, such as poly(butylene adipate-*co*-terephthalate) (PBAT) [2, 3, 4, 5, 6, 7], poly(-butylene succinate) (PBS) [8, 9], polycaprolactone (PCL) [10, 11, 12, 13], and polylactic acid (PLA) [14, 15].

Previous works report that 60% blending of PCL or PBAT improves TPS tensile strength ∼20 MPa and elongation at break more than 500% [2, 12]. TPS contributes to blend modulus as observed by Matzinos et al. [12] and the component ratio influences blend morphology [2, 11, 12]. Blends containing up to 50% TPS exhibited a matrix-dispersed phase morphology in which flexible polymers contributed to the continuous matrix and TPS to the dispersed phase. V-type crystalline structures were observed via XRD after extrusion melt mixing of TPS/biodegradable polyester blends [9]. Blend ratio was the primary determinant of crystalline peak intensity for both TPS and polyester. Mina et al. [13] observed TPS/PCL blend crystallinity values between those of TPS (13%) and PCL (50%). TPS also influenced polyester component morphological and thermal properties. Nayak [5] and Wang et al. [8] results suggest that TPS starch can be a polyester nucleating agent, increasing glass-transition and crystallization temperatures of PBAT and PBS, respectively.

Studies on storage time effects on TPS/biodegradable polyester blend properties are rather limited [10, 13, 14]. During storage, the TPS component may undergo retrogradation (i.e. recrystallization), leading to brittleness [16, 17, 18, 19, 20, 21]. When stored above its glass-transition temperature, TPS starch chain mobility increases allowing them to rearrange into more ordered structures [18]. When stored above 50% relative humidity [19, 20, 22], TPS absorbs moisture due to its hydrophilic nature. Water is an effective starch plasticizer due to its small molecular size allowing hydrogen bonding with starch. Thus, water further facilitates TPS recrystallization.

TPS recrystallization can be observed using XRD and DSC techniques. Ottenhof and Farhat [18] observed that both storage moisture content and temperature influenced the type of crystalline structures in wheat starch TPS. Potato starch TPS sheet extrusion yielded process-induced E_h and V_h crystalline structures [20]. Within a few days of storage at 20 °C and 54% relative humidity, E_h-type crystallinity decreased and converted to V_h-type. Both V_h- and B-type crystallinity increased during storage. Pushpadass and Hanna [19] found that corn starch TPS sheets stored at 20 °C and 53% relative humidity for 3 days developed V_h- and B-type crystallinity. During storage, crystalline peaks became sharper and well-defined, indicating increased crystallinity.

Changes in crystallinity also affect tensile properties. In the study by van Soest and Knooren [20], V_h- and B-type crystallinity increased in potato starch TPS sheets, thereby strengthening and stiffening the material. The elongation at break decreased 50% (from 250 to 125%) after 60 days of storage. Tensile strength and secant modulus at 2% strain increased from <2 to ∼10 MPa and <5 to >15 MPa, respectively. This outcome was also observed by Pushpadass and Hanna [19]. After 120 days, elongation at break decreased at least 50% while tensile strength increased 30%. Averous et al. [10] reported that blending with PCL reduced changes in TPS tensile properties.

Changes in crystallization behavior and mechanical properties may limit the service life of TPS blend systems. Environmental conditions in the warehousing, distribution, and end user storage pose challenges for TPS and TPS blend production because of inevitable effects on material properties. Thus, this study focused on monitoring the magnitude of TPS/PBAT film property changes during retention. This study specifically investigated blend ratio and low-humidity storage time effects on the morphological, thermal, and mechanical properties of TPS/PBAT blend films.

2. Materials and methods

2.1. Raw materials

Cassava starch (16% amylose content and 13.2% moisture content) and industrial grade glycerol (99.5% purity) were purchased from Tongchan (Thailand) and Siam Chemicals Solutions (Thailand), respectively. PBAT (Ecoflex®F blend C1200) was supplied by BASF (Germany). Magnesium nitrate (99.0% purity) used for saturated salt solution preparation for conditioning TPS/PBAT film samples was obtained from Ajax (Australia).

2.2. Pellet extrusion

2.2.1. TPS preparation

Cassava starch:glycerol weight ratio of 100:35 was pre-mixed with an all-purpose planetary mixer for 15 min via an auxiliary feeder (LHDFD1-130718, Labtech

Engineering, Thailand) with a screw speed of 20 rpm. The mixture was then fed into a co-rotating, fully intermeshing twin-screw extruder (LTE-20-40, Labtech Engineering) with a screw diameter of 20 mm and screw-length to diameter ratio (L/D) of 40:1. TPS pellets were prepared using an extrusion screw speed of 180 rpm with a temperature range of 80−150 °C. The extrudates were cut into 2.5 mm lengths with a pelletizer (LZ-120, Labtech Engineering).

2.2.2. *TPS/PBAT blend preparation*

TPS was then blended with virgin PBAT at 20, 40, and 60 wt% (i.e., T60/P40, T40/P60, and T20/P80) using a twin-screw extruder at a screw speed of 180 rpm and temperature of 120−150 °C. For the control sample, virgin PBAT was extruded using conditions similar to that of the TPS/PBAT blends (i.e. PBAT).

2.3. TPS/PBAT film preparation

TPS/PBAT blends with varied ratios were dried at 45 °C for 1 day. The films were produced by blown film extrusion using a single screw extruder (LE-25-30/C equipped with LF-400, Labtech Engineering) with a screw diameter of 25 mm and an L/D ratio of 30:1. Extrusion was performed at 150−190 °C with a screw speed of 35−44, a die temperature of 140−160 °C, a blow-up ratio of 3.0−3.5 and a draw-down ratio of 5.0−6.5. Obtained film samples were kept in an aluminum foil bag to prevent moisture loss or uptake and stored at room temperature (30 °C).

2.4. Characterization and testing

2.4.1. *Scanning electron microscopy*

Scanning electron microscopy (SEM) (LSMP-100, JEOL, Japan) revealed TPS/ PBAT film morphology. A rectangular sample was fragmented during submersion in liquid nitrogen. The fragmented film cross section was vertically positioned upwards on an aluminum stub. The sample was subsequently sputter-coated with gold. The continuous phase component of the TPS/PBAT films was determined by selectively extracting TPS using a 6 N hydrochloric acid solution for 3 hrs [23]. SEM images were taken at 10 kV with a working distance of 7.5 nm.

2.4.2. *Tensile testing*

The ASTM D882-02 [24] determined TPS/PBAT film tensile properties in the machine direction orientation using a universal testing machine (Model 5965, Instron, USA), with a grip separation distance of 50 mm and cross head speed of 500 mm/ min. The film was cut (2.5 cm × 10.0 cm) and conditioned at 52% RH and 25 °C for

2 days prior to tensile measurements. The tensile properties were measured at initial and after 3-month storage.

2.4.3. X-ray diffraction

X-ray diffraction (XRD) patterns of TPS/PBAT films were analyzed with a Bruker D8 Advance. Samples were scanned at diffraction angles (2θ) of $5-40°$ and a scan rate of $0.02°$/s [25]. XRD characterization of TPS/PBAT films was performed at initial and after 3-month storage. The peaks were determined using MDI Jade Version 5.0 software (USA).

2.4.4. Differential scanning calorimetry

Thermal transitions of TPS/PBAT blends were determined by differential scanning calorimetry (DSC) (Mettler Toledo DSC822, Switzerland) using film samples (~ 5 mg) placed inside 40-μL aluminum pans. According to ASTM D3418-03 [26], heating and cooling rates were both set at 10 °C/min. Samples were heated from −80 to 240 °C and cooled from 240 to −80 °C in a nitrogen atmosphere. Note that thermogravimetric analysis of TPS was performed to determine the onset temperature of thermal decomposition, which occurred at ~ 275 °C, prior to selecting the maximum temperature for DSC measurements. DSC analysis of TPS/PBAT films was performed at different storage times ($0-3$ months). TPS and PBAT component melting enthalpies (ΔH_f) in TPS/PBAT films obtained during the first heating scan were calculated using Eq. (1), where ΔH_m is the melting enthalpy and w is the component weight fraction in the blend [27].

$$\Delta H_f = \Delta H_m / w \ x \ 100 \qquad (1)$$

The degree of PBAT component crystallinity (χ_c) in TPS/PBAT films was calculated using Eq. (2) [27], where ΔH_m^{*} is the melting enthalpy of 100% crystalline PBAT ($\Delta H_m^{*} = 114$ J/g):

$$\chi_{c,PBAT} = \Delta H_f \big/ \Delta H_m* \ x \ 100 \qquad (2)$$

2.4.5. Dynamic mechanical analysis

Glass-transition temperatures of TPS/PBAT blend films were determined using dynamic mechanical analysis (DMA, Eplexor GaboQualimeter, Germany) in tension mode with a 1 Hz frequency, 0.2 N static load, and 0.1 N dynamic load. A film sample was cut into 10 mm × 50 mm rectangles. Maximum and static strain was set to 1.5% and 0.5%, respectively. Measurements were taken at temperatures from −80 to 50 °C at a heating rate of 2 °C/min. Tan delta (*tan δ*) was evaluated as a function of temperature to determine TPS/PBAT film glass-transition temperatures.

3. Results and discussion

3.1. Effect of blend ratio on properties of TPS/PBAT films at initial stage

3.1.1. TPS/PBAT blend morphology

Comparisons between TPS/PBAT blend, TPS, and PBAT SEM micrographs are illustrated in Fig. 1. Cryogenic fragmentation distorted the PBAT surface cross-section while TPS showed smoother fracturing. However, TPS is both more brittle and breakable than PBAT. Miscibility limitations between PBAT and TPS produced a matrix-dispersed phase type in the TPS/PBAT blend films, with the dispersed TPS phase occurring in the PBAT matrix.

Cavities previously occupied by the dispersed TPS phase became detached during fragmentation in TPS/PBAT films with blend ratios of 20/80 and 40/60 (Fig. 1). Cavity size decreased from approximately 0.3−4.5 μm to 0.2−1.3 μm when increasing TPS loading content from 20 to 40 wt%. Increasing TPS content improved the dispersion homogeneity of the TPS/PBAT blends. A similar trend is also reported by Wei et al. [2] for TPS/PBAT blends containing 10−30% of thermo-plastic potato starch.

Increasing the TPS:PBAT blend ratio from 40/60 to 60/40 increased the size of dispersed TPS phases, becoming the dominant structure. TPS was selectively removed from the TPS/PBAT film via an aqueous solution of hydrochloric acid (6 N) in order to determine dispersed phase homogeneity in the continuous PBAT matrix. The PBAT continuous matrix still remained (Fig. 2) even in the blend containing only 40% of PBAT due to greater flexibility and ability to be stretched in the machine direction during film blowing process.
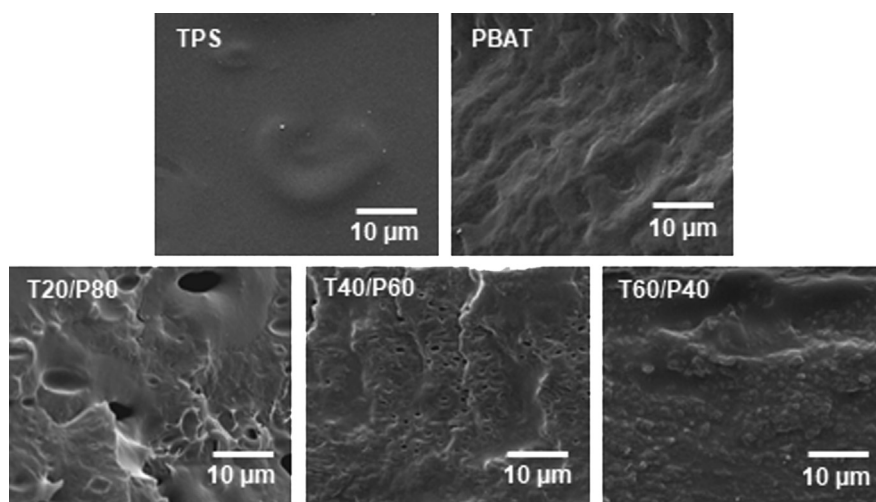
Fig. 1. SEM micrographs of TPS/PBAT films compared with those of TPS and PBAT taken at initial storage (0 month).
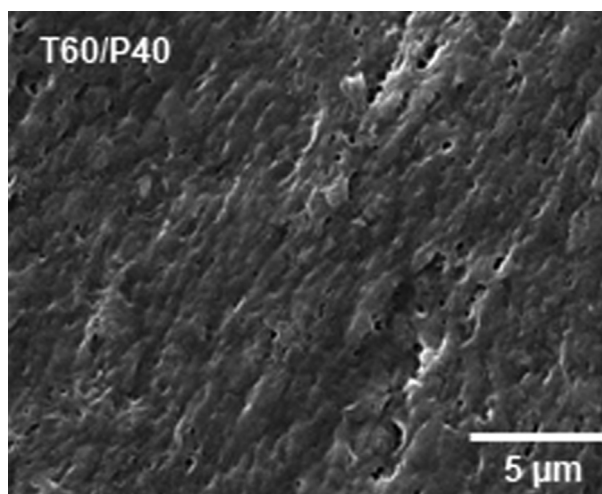
Fig. 2. SEM micrograph of T60/P40 film surface after selective TPS removal at initial storage (0 month).
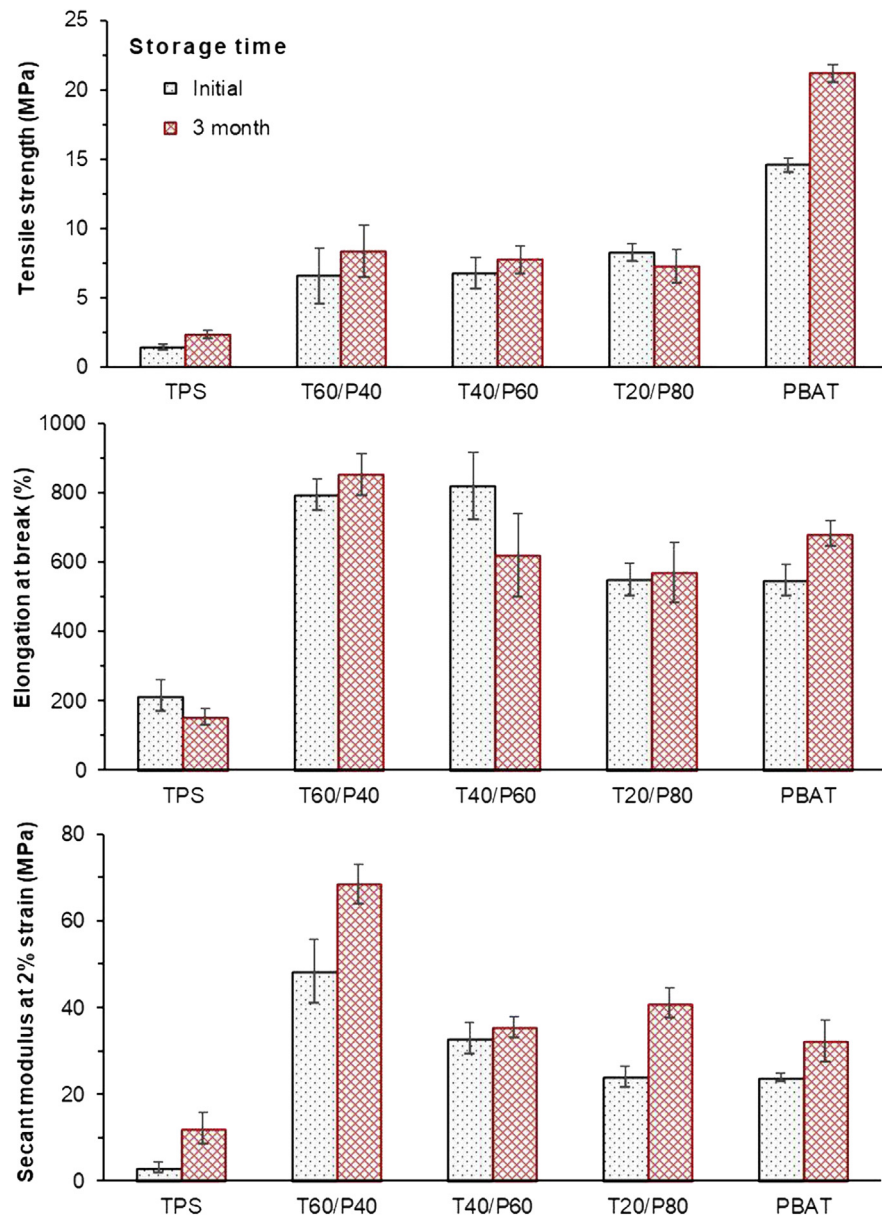
3.1.2. Tensile properties

Tensile property comparisons at initial storage of the TPS/PBAT films, TPS, and PBAT are shown in Fig. 3. TPS tensile strength, elongation at break, and secant modulus at 2% strain were 1.5 MPa, 216%, and 3.2 MPa, respectively, agreeing with the results of van Soest and Knooren [20]. PBAT showed greater tensile strength, elongation at break, and secant modulus at 2% strain (14.6 MPa, 794% and 48.4 MPa, respectively) being consistent with work of Mohanty and Nayak [28]. TPS blending led to reduced PBAT tensile strength, elongation at break, and secant modulus at 2% strain to 6.6−8.3 MPa, 547−819%, and 23.9−33.0 MPa, respectively. Specifically, increasing the TPS:PBAT ratio from 20/80 to 40/60 resulted in decreased tensile strength, elongation at break, and secant modulus at 2% strain from 8.3 to 6.8 MPa, 819 to 551%, and 33.0 to 24.0 MPa, respectively. However, increasing the TPS:PBAT ratio further to 60/40 had no significant effect on TPS/PBAT blend tensile properties. A decrease in TPS/PBAT blend elongation at break with increases in TPS content agrees with Wei et al. [2] research results.

3.1.3. Microstructures

The crystalline patterns of native cassava starch, TPS, PBAT, and TPS/PBAT films at initial storage are shown in Fig. 4. Native cassava starch has an A-type crystal structure with characteristic peaks at 2θ of 15.2°, 17.2°, 18.1°, and 22.8° as already reported by Thipmanee and Sane [29]. After starch plasticization with glycerol through extrusion, the A-type pattern of native cassava starch disappeared, clearly revealing new E_h-type and V_h-type pattern diffraction peaks at 2θ of 11.9° and 18.5°, and 2θ of 13.1°, 20.0°, and 24.7°, respectively, as previously established by van Soest et al. [30]. Concerning PBAT crystals, strong diffraction appeared at 2θ of 16.3°, 17.7°, 20.5°, 23.4°, and 25.3°, similarly found by Li et al. [31].

Fig. 3. The effect of blend ratio and storage time on TPS/PBAT blend tensile properties compared with those of TPS and PBAT.

For TPS/PBAT films with varied blend ratios, the V_h-type pattern of TPS overlapped with that of PBAT crystals. Regarding the addition of 20 wt% TPS in TPS/PBAT film, the strong PBAT diffraction peaks shift to higher positions at 16.5°, 17.9°, 20.7°, 23.5°, and 25.5° 2θ, indicating more ordered packing of the crystalline PBAT phase. This result suggests that TPS effectively functions as a nucleating agent for PBAT. However, the highly ordered structure of PBAT in the blend film significantly decreased when reducing PBAT content (i.e., T40/P60 and T60/P40), observable from the broadened peaks and the downward shift of the diffraction position.
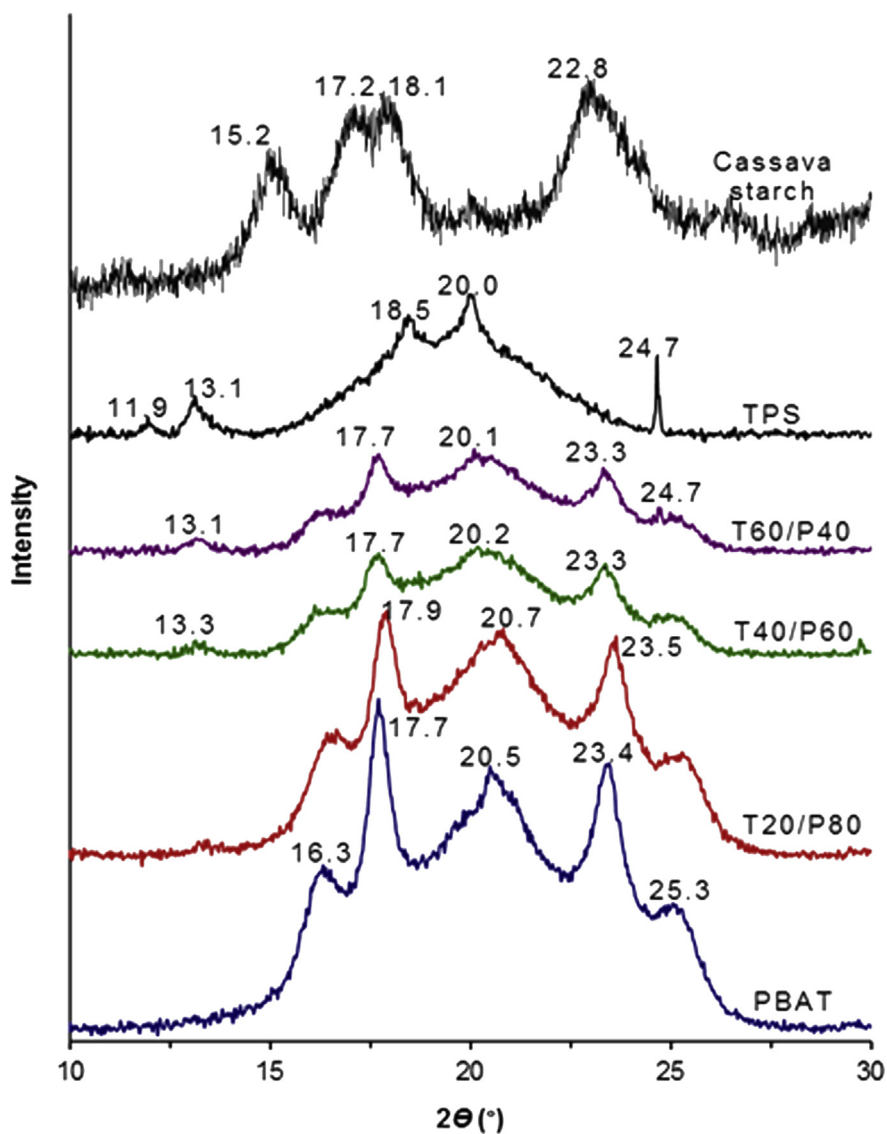
Fig. 4. X-ray diffraction patterns of TPS, PBAT and TPS/PBAT films at initial storage (0 month).

Remarkably, the TPS/PBAT blend ratios of 40/60 and 60/40 show similar broad diffraction patterns with the coexistence of both crystalline TPS and PBAT phases. These reflected the thorough dispersion of each polymeric phase in the blend system [32], as confirmed by the morphology observed in SEM micrographs (Fig. 1).

3.1.4. Thermal properties

In this work, the DSC technique was applied to trace the melting and crystallization temperatures of TPS and PBAT in the blend system, as illustrated in Fig. 5. TPS was molten at 147 °C, possibly attributed to the V_h-type crystal, whereas PBAT exhibits two endothermic peaks at 46 and 115 °C, corresponding to (i) the small crystal
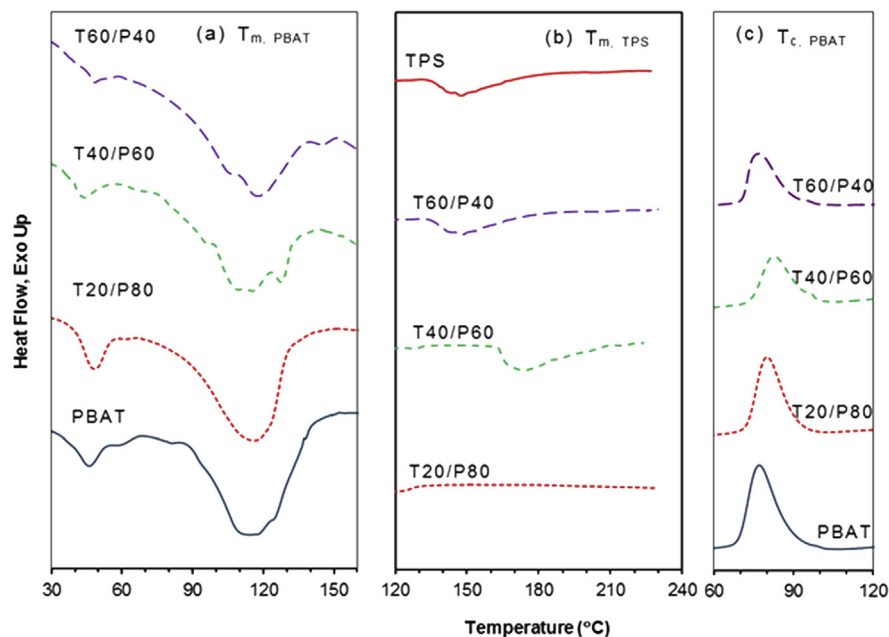
Fig. 5. DSC thermograms of heating (a and b) and cooling (c) scans of TPS/PBAT blends, as compared with neat TPS and PBAT at initial storage (0 month).

domain of the poly(butylene adipate) (PBA) segment [28] and (ii) crystalline poly(-butylene terephthalate) (PBT) segment [33]. The total degree of crystallinity (χ_c) of PBAT was 23%. For TPS/PBAT films, when TPS content increased, the endotherms of PBA and PBT segments gradually declined whereas the melting peak of TPS sharpened, as shown in Fig. 5. Furthermore, increasing the TPS/PBAT ratio led to decreased TPS melting temperatures.

Regarding crystallization behavior, only PBAT presented crystallization temperature (T_c) during cooling scan. The T_c of PBAT increased from 77 to 80 and 83 °C after blending with 20 and 40% of TPS, respectively. The increase in T_c of PBAT with increasing TPS content may be the result of starch acting as nucleating sites for PBAT. A similar trend was also observed in the study of Nayak [5]. However, this trend was not observed for the T60/P40 blend, possibly because substantial amounts of TPS and TPS dispersed phase agglomeration may hinder the movement and crystallization of PBAT chains [34, 35].

Additionally, the glass-transition temperature (T_g) of PBAT obtained from DSC analysis occurred at −33 °C. The T_gs of PBAT-rich phase in TPS/PBAT blends were observed between −31 and −30 °C. The increase in the PBAT-rich phase T_g compared to that of PBAT indicates that TPS restrains PBAT chains movement in the amorphous region. Similar results were observed in the studies of Nayak [5]. Unfortunately, the T_gs of TPS and the TPS-rich phase in TPS/PBAT blends were not observed from DSC analysis, possibly due to interference from the PBA melting transition crystalline structure of PBAT.

The TPS and PBAT component T_gs in their blends at initial stage were also determined using DMA technique (Fig. 6). PBAT showed a T_g of −24 °C, and after blending with TPS, PBAT T_g increased by ∼1−3 °C. For T40/P60 and T60/P40 blends, their *tan δ* curves were similar and the peaks of PBAT and starch-rich components partially overlapped. For the T20/P80 blend, only a single prominent peak occurred at −21 °C, corresponding to the glass transition of PBAT, without the peaks of glycerol-rich and starch-rich phases due to the small quantity of TPS present in the blend.

3.2. Effect of storage time on properties of TPS/PBAT films

3.2.1. Tensile properties

TPS/PBAT film tensile property changes during storage compared with those of TPS and PBAT films are shown in Fig. 3. Tensile strength increased for all samples after 3 months of storage except for the T20/P80 blend. TPS and PBAT films experienced significant tensile strength increases from 1.5 to 2.4 MPa (60%) and 14.6−21.2 MPa (45%), respectively. Similar trends were also observed for TPS/PBAT blends with tensile strengths increasing from 6.8 to 7.8 MPa and 6.6−8.4 MPa for T40/P60 and T60/P40 blends, respectively.

Secant modulus at 2% strain also increased after 3 months of storage for all films except for the T20/P80 blend. TPS and PBAT secant moduli increased from 3.2 to 12.2 MPa and 48.4−68.5 MPa, respectively. The secant moduli of T40/P60 and T60/P40 blends increased from 24.0 to 41.0 MPa and 23.9−32.3 MPa,
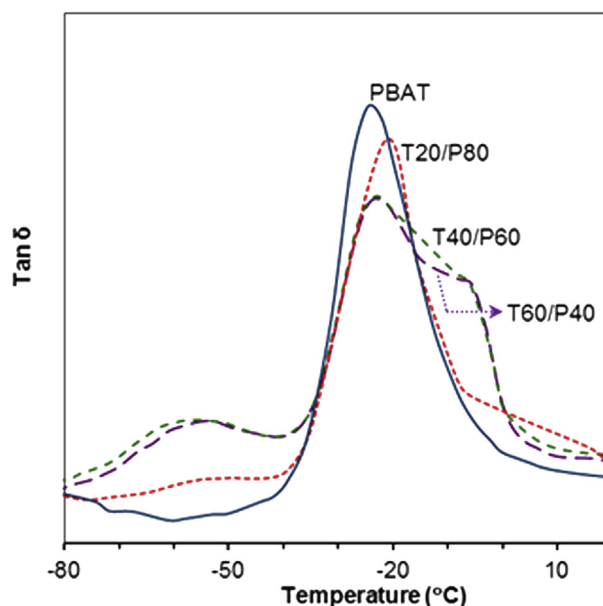
Fig. 6. PBAT and TPS/PBAT film glass-transition temperatures at initial storage (0 month) determined from *tan δ* curves using DMA.

respectively. The secant modulus at 2% strain of the T20/P80 blend, however, remained unchanged and agreed with the tensile strength trend.

Elongation at break of TPS and T20/P80 blend decreased from 216 to 155% and 819 to 620%, respectively, after 3 months of storage. PBAT and T40/P60 blend break points, however, remained approximately the same. T60/P40 blend elongation at break increased from 547 to 682%. The results suggest that T60/P40 blend flexibility increases with storage time, possibly due to glycerol migration from the TPS to the PBAT continuous phase.

Increased TPS tensile strength and secant modulus at 2% strain along with reduced elongation at break suggest continued hardening and embrittlement with storage duration, the result of free volume reduction and starch chain recrystallization [19, 20, 22]. TPS/PBAT blend tensile strength and secant modulus at 2% strain increments were smaller compared to those of neat TPS and PBAT, possibly due to blend component interference preventing individual components to recrystallize. Not only did T60/P40 blend tensile strength and secant modulus at 2% strain increase with storage time, but also its elongation at break. Shi et al. [36] suggests that glycerol migrates from the crystalline region to the amorphous region during TPS recrystallization. Therefore, glycerol may be migrating from the T60/P40 blend TPS phase, thereby plasticizing the continuous phase (i.e., PBAT phase), and ultimately increasing both blend flexibility and toughness over time. Furthermore, PBAT blending may reduce the increment of TPS secant modulus at 2% strain during storage.

3.2.2. Microstructures

After 3 months of storage, TPS, PBAT, and TPS/PBAT films were characterized to determine crystalline pattern changes. V_h-type peaks sharpened at 2θ of 17.7° and 20.0° and intensity increased dramatically at 2θ of 24.7° for TPS (Fig. 7). The increment of V_h-type crystalline structure during storage suggests a starch phase recrystallization within the blend system, as reported by Shi et al. [36]. PBAT crystal diffractions at 2θ of 16.3°, 17.7°, 20.5°, and 23.4° became more intense, implying enlarged PBAT crystallites.

T20/P80 showed a similar change in diffraction patterns to that of PBAT (Fig. 7), considering the crystalline PBAT and TPS blend phase changes. However, when TPS content was increased to 40−60 %, there were slight changes at 2θ of 17.7°, 20.0°, and 23.4° after TPS/PBAT film storage. These results indicate a low PBAT recrystallization rate in the blend system. This may be the result of well-dispersed TPS in the PBAT matrix obstructing PBAT recrystallization during storage. At 40 % TPS, the diffraction at 2θ of 24.7° from the TPS phase after 3-month storage was observed, but was not as intense as the T60/P40 blend or neat TPS. Increases in TPS, PBAT, and TPS/PBAT film crystallinity after 3-month storage led to tensile
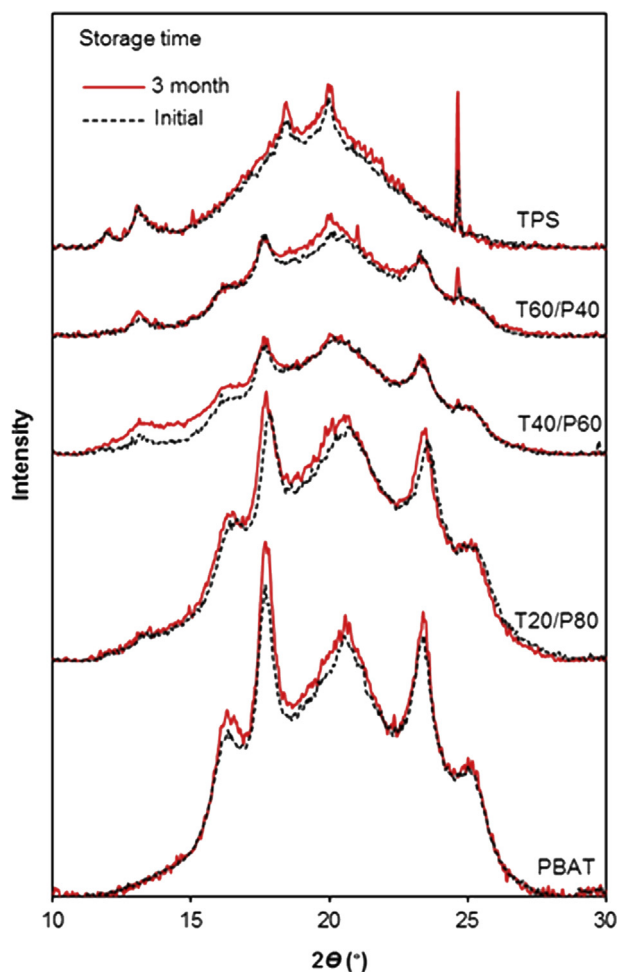
Fig. 7. TPS, PBAT, and TPS/PBAT film X-ray diffraction patterns at initial stage and after 3-month storage.

strength and secant modulus at 2% strain increments, as well as a reduction in elongation at break.

3.2.3. Thermal properties

Fig. 8 shows a DSC thermal transition overlay for different films stored at room temperature between 0 and 3 months. After 3 months, the T_m of the starch-rich phase in TPS increased from 147 to 182 °C (Fig. 8b) and its corresponding melting enthalpy, ΔH_f, increased from 26 to 117 J/g. For the T20/P80 blend, the melting endotherm of TPS was observed at 216 °C with ΔH_f of 66 J/g for the same period. The T_m of starch-rich phase in the T40/P60 blend increased from 174 to 187 °C after 3 months, the melting endotherm became sharper, and the ΔH_f also increased. Similar trends were also observed for the T60/P40 blend. The increase in starch-rich phase ΔH_f implies a crystallinity increase in TPS/PBAT blends, agreeing with XRD results
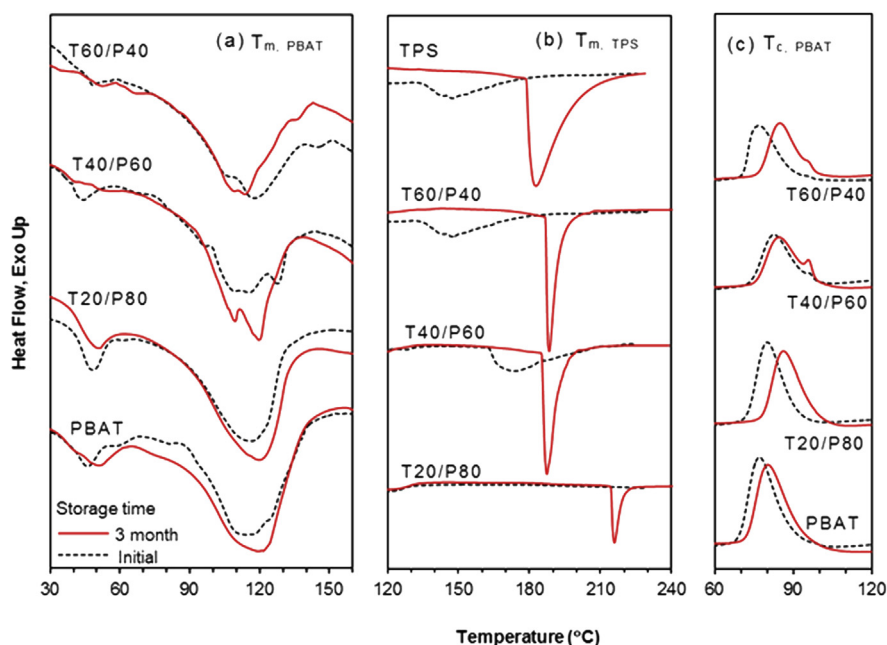
Fig. 8. Heating scan (a and b) and cooling scan (c) DSC thermograms for TPS, PBAT, and TPS/PBAT blends at initial stage and after 3-month storage.

(Fig. 7). Similar trends for the same time period were observed for the PBAT-rich phase in TPS/PBAT blends (Fig. 8a). For the T20/P80 blend, the χ_c of PBAT rich-phase increased slightly from 24 to 27% and its T_m increased from 116 to 119 °C. Crystallinity of the PBAT-rich phase also increased with storage time for the 40−60% PBAT blends and the melting peak narrowed with two distinct transition temperatures between 110 and 120 °C. These results suggest that PBAT undergoes recrystallization during storage, forming more ordered structures.

PBAT crystallization temperature (T_c) increased from 77 to 81 °C after 3 months of storage (Fig. 8c). A similar trend was also observed for TPS/PBAT blends. Large T_c increase for the PBAT-rich phase, up to 8 °C, was observed for T20/P80 and T60/P40 blends. However, the T40/P60 blend only experienced a small T_c increase of 2 °C after 3 months of storage. Furthermore, the small peak at ∼95 °C for TPS/PBAT blends containing 40−60% TPS, possibly indicates heterogeneous nucleation induced by the presence of starch molecules [5] which would agree with the previously mentioned splitting of PBAT-rich phase melting transitions.

The PBAT glass-transition temperatures determined from DSC analysis remained unchanged at ∼−33 °C after 3 months of storage. A similar trend also occurred for PBAT-rich phase T_gs in TPS/PBAT blends with the T_gs remaining between −30 and −29 °C.

DMA results (Fig. 9) illustrate the effect of storage time on TPS/PBAT film *tan* δ curves compared with that of PBAT. The PBAT *tan* δ peak remained at −24
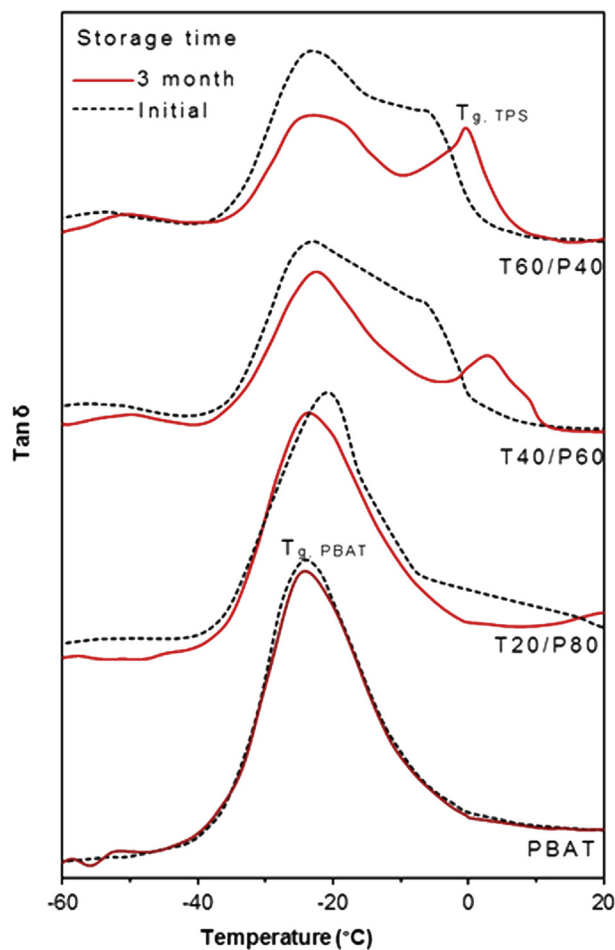
Fig. 9. *Tan δ* curves of TPS/PBAT films shown in comparison with those of PBAT at initial stage and after 3-month storage.

°C, revealing that PBAT T_g did not significantly change after 3 months of storage. After the same period, the PBAT-rich phase *tan δ* peak in the T20/P80 blend decreased from −21 to −24 °C. Two sharper individual peaks at −22 and 3 °C replaced the single broad peak of the T40/P60 blend, corresponding to PBAT-rich and starch-rich phase glass transitions, respectively. Both the T40/P60 and T60/P40 blend *tan δ* curves showed similar trends. The TPS-rich phase T_g increase observed for the T40/P60 and T60/P40 blends could be attributed to TPS-rich phase recrystallization [16] and glycerol loss from the TPS-rich phase. The TPS-rich phase T_g increment over 3 months of storage increased with decreasing TPS:PBAT ratios, possibly because a relatively larger proportion of glycerol migrated out of TPS-rich phase into PBAT-rich phase resulting in less glycerol content remained in the TPS-rich phase. However, glycerol migration from the TPS-rich phase did not significantly affect the PBAT-rich phase T_g possibly because PBAT-rich phase crystallinity increased with storage time as shown in XRD and DSC results (Figs. 7 and 8a).

4. Conclusions

TPS and PBAT were melt blended with varied weight ratios for a comparative study of morphological, mechanical, and thermal property changes after 3-month storage. At the initial stage, increasing TPS:PBAT ratios led to improved TPS dispersion in the PBAT matrix and decreased tensile strength, modulus, and flexibility of TPS/PBAT films. Increasing the TPS:PBAT ratio reduced the TPS melting transition while increasing the PBAT crystallization temperature. After storage for 3 months, TPS/PBAT film tensile strength and secant modulus at 2% strain increased due to TPS and PBAT recrystallization. However, the thorough dispersion of TPS limited PBAT phase recrystallization in TPS/PBAT films. The recrystallization of TPS V_h-type pattern was clearly evident when increasing the TPS:PBAT ratio. Moreover, the increase in T60/P40 blend flexibility with storage time was possibly caused by glycerol migrating from the TPS-rich phase to plasticize the PBAT continuous phase. The increment of T_g of the TPS-rich phase with storage time increased with decreasing TPS:PBAT ratios as a relatively larger proportion of glycerol migrated from the TPS-rich phase into the PBAT-rich matrix.

Declarations

Author contribution statement

Ray Anne Garalde: Performed the experiments; Analyzed and interpreted the data; Wrote the paper.

Ranumas Thipmanee, Piyawanee Jariyasakoolroj: Analyzed and interpreted the data.

Amporn Sane: Conceived and designed the experiments; Wrote the paper.

Funding statement

Competing interest statement

The authors declare no conflict of interest.

Additional information

No additional information is available for this paper.

References

[1] A.J.F. Carvalho, Starch: major sources, properties and applications as thermoplastic materials, in: S. Ebnesajjad (Ed.), Handbook of Biopolymers and Biodegradable Plastics, Elsevier, USA, 2013, pp. 129−152.

[2] D. Wei, H. Wang, H. Xiao, A. Zheng, Y. Yang, Morphology and mechanical properties of poly(butylene adipate-co-terephthalate)/potato starch blends in the presence of synthesized reactive compatibilizer or modified poly(butylene adipate-*co*-terephthalate), Carbohydr. Polym. 123 (2015) 275−282.

[3] R.P.H. Brandelero, M.V.E. Grossman, F. Yamashita, Effect of the method of production of the blends on mechanical and structural properties of biodegradable starch films produced by blown film extrusion, Carbohydr. Polym. 86 (2011) 1344−1350.

[4] N.M.C. da Silva, P.R.C. Correia, J.I. Druzian, F.M. Fakhouri, R.L.L. Fialho, E.C.M.C. de Albuquerque, PBAT/TPS composite films reinforced with starch nanoparticles produced by ultrasound, Int. J. Polym. Sci. (2017) 1−10.

[5] S.K. Nayak, Biodegradable PBAT/starch nanocomposites, Polym. Plast. Technol. Eng. 49 (2010) 1406−1418.

[6] M.O. Reis, J.B. Olivato, J. Zanela, F. Yamashita, M.V.E. Grossmann, Influence of microcrystalline cellulose in thermoplastic starch/polyester blown films, Polímeros 27 (2017) 129−135.

[7] P.G. Seligra, L.E. Moura, L. Famá, J.I. Druzian, S. Goyanes, Influence of incorporation of starch nanoparticles in PBAT/TPS composite films, Polym. Int. 65 (2016) 938−945.

[8] W. Wang, G. Zhang, W. Zhang, W. Guo, J. Wang, Processing and thermal behaviors of poly(butylene succinate) blends with highly-filled starch and glycerol, J. Polym. Environ. 21 (2013) 46−53.

[9] J. Li, X. Luo, X. Lin, Y. Zhou, Comparative study on the blends of PBS/thermoplastic starch prepared from waxy and normal corn starches, Starch/Stärke 65 (2013) 831−839.

[10] L. Averous, L. Moro, P. Dole, C. Fringant, Properties of thermoplastic starch blends: starch-polycaprolactone, Polymer 41 (2000) 4157−4167.

[11] G. Li, B.D. Favis, Morphology development and interfacial interactions in polycaprolactone/thermoplastic-starch blends, Macromol. Chem. Phys. 211 (2010) 321−333.

[12] P. Matzinos, V. Tserki, A. Kontoyiannis, C. Panayiotou, Processing and characterization of starch/polycaprolactone products, Polym. Degrad. Stabil. 77 (2002) 17−24.

[13] H.J. Mina, G.A. Valadez, T.T. Toledano, Estudio Fisicoquímico de mezclas de almidón termoplástico (TPS) y policaprolactona (PCL), Biotecnología en el Sector Agropecuario y Agroindustrial - Edición Especial 2 (2013) 31−40.

[14] O.H. Arroyo, M.A. Huneault, B.D. Favis, M.N. Bureau, Processing and properties of PLA/thermoplastic starch/montmorillonite nanocomposites, Polym. Compos. 31 (2010) 114−126.

[15] P. Müller, B. Imre, J. Bere, J. Móczó, B. Pukánszky, Physical ageing and molecular mobility in PLA blends and composites, J. Therm. Anal. Calorim. 122 (2015) 1423−1433.

[16] L. Famá, S. Goyanes, L. Gerschenson, Influence of storage time at room temperature on the physicochemical properties of cassava starch films, Carbohydr. Polym. 70 (2007) 265−273.

[17] K. Kohyama, J. Matsuki, T. Yasui, T. Sasaki, A differential thermal analysis of the gelatinization and retrogradation of wheat starches with different amylopectin chain lengths, Carbohydr. Polym. 58 (2004) 71−77.

[18] M.−A. Ottenhof, I. Farhat, Starch retrogradation, Biotechnol. Genet. Eng. Rev. 21 (2004) 215−228.

[19] H.A. Pushpadass, M.A. Hanna, Age-induced changes in the microstructure and selected properties of extruded starch films plasticized with glycerol and stearic acid, Ind. Eng. Chem. Res. 48 (2009) 8457−8463.

[20] J.J.G. van Soest, N. Knooren, Influence of glycerol and water content on the structure and properties of extruded starch plastic sheets during aging, J. Appl. Polym. Sci. 64 (1997) 1411−1422.

[21] Y. Zhang, C. Rempel, Retrogradation and antiplasticization of thermoplastic starch, in: A.Z. El-Sonbati (Ed.), Thermoplastic Elastomers, InTech, Croatia, 2012, pp. 117−134.

[22] H. Schmitt, A. Guidez, K. Prashantha, J. Soulestin, M.F. Lacrampe, P. Krawczak, Studies on the effect of storage time and plasticizers on the structural variations in thermoplastic starch, Carbohydr. Polym. 115 (2015) 364−372.

[23] M.A. Huneault, H. Li, Preparation and properties of extruded thermoplastic starch/polymer blends, J. Appl. Polym. Sci. 126 (2012) E96−E108.

[24] ASTM D882-02, Standard Test Method for Tensile Properties of Thin Plastic Sheeting, American Society for Testing and Materials, Philadelphia, 2002.

[25] K.M. Dang, R. Yoksan, Development of thermoplastic starch blown film by incorporating plasticized chitosan, Carbohydr. Polym. 115 (2015) 575−581.

[26] ASTM D3418-03, Standard Test Method for Transition Temperatures and Enthalpies of Fusion and Crystallization of Polymers by Differential Scanning Calorimetry, American Society for Testing and Materials, Philadelphia, 2003.

[27] F. Chivrac, Z. Kadlecová, E. Pollet, L. Avérous, Aromatic copolyester-based nano-biocomposites: elaboration, structural characterization and properties, J. Polym. Environ. 14 (2006) 393−401.

[28] S. Mohanty, S.K. Nayak, Biodegradable nanocomposites of poly(butylene adipate-co-terephthalate) (PBAT) with organically modified nanoclays, Int. J. Plast. Tech. 14 (2010) 192−212.

[29] R. Thipmanee, A. Sane, Effect of zeolite 5A on compatibility and properties of linear low-density polyethylene/thermoplastic starch blend, J. Appl. Polym. Sci. 126 (2012) E251−E258.

[30] J.J.G. van Soest, S.H.D. Hulleman, D. de Wit, J.F.G. Vliegenthart, Crystallinity in starch bioplastics, Ind. Crops Prod. 5 (1996) 11−22.

[31] G. Li, S. Shankar, J.−W. Rhim, B.−Y. Oh, Effects of preparation method on properties of poly(butylene adipate-co-terephthalate) films, Food Sci. Biotechnol. 24 (2015) 1679−1685.

[32] D. Campbell, R.A. Pethrick, J.R. White, X-ray diffraction, in: Polymer Characterization: Physical Techniques, second ed., Stanley Thornes, UK, 2000, pp. 194−236.

[33] R. Herrera, L. Franco, A. Rodríguez-Galan, J. Puiggalí, Characterization and degradation behavior of poly(butylene adipate-*co*-terephthalate), J. Polym. Sci. Part A: Polym. Chem. 40 (2002) 4141−4157.

[34] G.−S. Jang, W.−J. Cho, C.−S. Ha, Crystallization behavior of polypropylene with or without sodium benzoate as a nucleating agent, J. Polym. Sci. Part B: Polym. Phys. 39 (2001) 1001−1016.

[35] A.G. Simanke, A.P. de Azeredo, C. de Lemos, R.S. Mauler, Influence of nucleating agent on the crystallization kinetics and morphology of polypropylene, Polímeros 26 (2016) 152−160.

[36] R. Shi, Q. Liu, T. Ding, Y. Han, L. Zhang, D. Chen, W. Tian, Ageing of soft thermoplastic starch with high glycerol content, J. Appl. Polym. Sci. 103 (2007) 574−586.